Title

The effects of process variations on residual stress in laser peened 7049 T73 aluminum alloy

Journal

Materials Science and Engineering A-Structural Materials Properties Microstructure and Processing, 349(1-2)

ISSN

0921-5093

Authors

Rankin, Jon E
Hill, Michael R
Hackel, Lloyd A

Publication Date

2003-05-01

Peer reviewed

The effects of process variations on residual stress in laser peened 7049 T73 aluminum alloy

Jon E. Rankin and Michael R. Hill[1]
Mechanical and Aeronautical Engineering Department,
University of California, Davis, CA USA

Lloyd A. Hackel,
Laser Science and Technology Program,
Lawrence Livermore National Laboratory, Livermore, CA USA

Accepted for publication in
Materials Science and Engineering A
Submitted March, 2002
Revised September, 2002

Abstract

This paper reports measurements of the distribution of residual stress with depth from the surface in laser peened coupons made of a high-strength aluminum alloy. Residual stresses were measured using slitting (also known as the crack compliance method). Measurements were made on several coupons to: compare laser peening (LP) and shot peening residual stresses; ascertain the influence of LP parameters on residual stress; determine whether tensile residual stress existed outside the peened area; assess the variation of residual stress with in-plane position relative to the layout of the laser spots used for peening; and, determine the importance of a uniform spatial distribution of laser energy within the spot. Residual stress 0.1 mm from the surface due to LP and shot peening were comparable and the depth of the compressive stress for LP was far greater than for shot peening. Variations of most LP parameters did not significantly alter residual stress at shallow depths, but greater laser energy and larger layer overlap increased residual stress at depths between 0.2 and 0.6 mm from the surface. Residual stresses adjacent to the peened area were found to be compressive. Decreased levels of surface residual stress were found when laser spots had a non-uniform distribution of laser intensity.

[1] Corresponding author, Mechanical and Aeronautical Engineering Department, University of California, Davis, CA 95616, USA, (530)754-6178, (530)752-4158 (FAX), mrhill@ucdavis.edu

Introduction

Laser peening is an emerging surface treatment, capable of imparting compressive surface residual stress and thereby improving the resistance of components to fatigue failure. While the general mechanical concept is similar to conventional shot peening, laser peening (LP) offers certain advantages. First, LP leaves a more desirable surface than does shot peening (SP). In stainless steel, LP has a reduced occurrence of strain-induced phase transformation compared with SP, thereby leaving a surface more resistant to corrosive attack [1]. In aluminum, LP may also leave an improved surface, which would reduce the occurrences of surface lapping, folds, and other undesirable features that occur with SP [2]. The improved surface condition should therefore result in improved resistance to crack initiation. Second, while LP and SP create residual stresses of similar magnitude, the compressive stresses extend far deeper from the surface for LP [3], thereby offering improved resistance to the growth of near-surface, macroscopic cracks. These two characteristics can therefore lead to significant improvements in the fatigue life of treated components.

These potential advantages of LP point to the need to further understand the effects of this process for a wide range of materials and geometry. This is especially the case since recent advances in laser science and technology [4-6] have enabled LP to become cost effective for a wider variety of components. This work presents measurements of the distribution (or, "profile") of LP-induced residual stress with distance from the surface under a variety of processing conditions for a high strength aluminum alloy used in aerospace structure (7049 T73). We refer to measurements of residual stress throughout

the paper; technically, however, released strain was measured while residual stress was computed.

While potential improvements in fatigue life make LP an attractive process, its adoption will likely depend on verifying its performance relative to competing surface treatments. Because SP is the most commonly used surface residual stress treatment for aerospace structure, the effects of LP are often compared to the effects of SP (e.g., [3, 6]). Considering that the beneficial effects of either type of peening on fatigue life are primarily due to the near-surface residual stress field, the first objective of this paper is to compare the residual stress profile produced by LP to that produced by SP in 7049 T73 aluminum.

The residual stress profile due to LP is influenced by several process parameters. One basic process parameter is the fluence of the laser pulse (laser energy per spot area). A second important parameter is the size of the laser spot. A third important parameter is the number layers of peening applied to a component and, for multi-layer peening, a fourth important parameter is the spatial offset, or "overlap", from one peening layer to another. These parameters have been investigated to various degrees in a number of materials. Smith et al [7] reported the effects of fluence and the number of peening layers on the residual stress profile in Ti-6Al-4V. Peyre and Fabbro, with various co-authors, have studied the effects of fluence and the number of peening layers on the residual stress profile in aluminum alloys [3, 8], as well as the effect of layer overlap on *surface* residual stress in stainless steel [9]. Despite these efforts, the influences of process parameters, particularly spot size and layer overlap, on the resulting residual stress profiles produced by LP are not wholly understood. Therefore, the second objective of this paper is to

assess the variation of the LP-induced residual stress profile in 7049-T73 aluminum with changes in laser energy, laser spot size, and layer overlap.

Surface treatments like LP are most often applied to specific, highly stressed locations of a component. Typical application areas include mechanical joints, notches, fillets, and other abrupt changes in cross section. While compressive surface residual stress is imparted within a peened area, tensile surface residual stress may result outside the peened area, which may have deleterious effects on component performance. To determine whether tensile surface residual stress exists adjacent to the peened region, the third objective is to examine the in-plane variation of the residual stress profile adjacent to a laser peened area.

The scale of laser peening is large compared with the mechanisms of fatigue crack initiation, and this may have an influence on the ability of LP to improve fatigue life. Spatial, in-plane variations of residual stress induced by shot peening may be expected to be on a scale of approximately 0.1 mm, due to the small size and small amounts of penetration of the shot [2]. In contrast, the LP spot size is on the order of 3 to 10 mm, so that relatively large-scale, in-plane variations of residual stress may exist and may influence potential fatigue life improvements. For this reason, the fourth objective of this paper is to investigate the in-plane variation of the residual stress profiles within a laser peened region.

Despite efforts to the contrary, a potential exists for laser optics to become misaligned, or otherwise degraded, resulting in a non-uniform spatial distribution of energy within the laser spot. While such problems can be detected on-line [4] and subsequently corrected, it is nevertheless important to investigate the effect of laser spot

variation on the resulting residual stress profiles. The final objective is therefore to examine the in-plane variations of the residual stress profiles for a surface peened with intentionally altered laser spots, and to compare the residual stresses to those occurring for a normally peened surface.

Methods

The objectives described above were addressed by measuring residual stress in a series of coupons peened in various ways. Residual stresses were measured by relaxation, using the slitting method (also called the compliance method or the crack compliance method) [10]. In the following section, the slitting method is presented in general and then experimental details are provided for the present set of experiments. A set of seven peened samples and fifteen measurement locations is then described, which together address the objectives just stated.

The Slitting Method

The general procedure for the slitting method is to gradually extend a slit into the specimen surface and measure near-slit strain as a function of slit depth. Strain released perpendicular to the slit was measured using a metallic foil gage placed near the slit (Figure 1). The slits were cut incrementally in depth using wire electrical discharge machining (EDM). The strain versus depth data were then used to compute the variation of the pre-slit residual stress component normal to the slit face with depth from the surface (i.e., the stress profile).

Solving for the residual stress profile from measured strain data requires the solution of an elastic inverse problem. The inverse problem is solved by first representing

the unknown residual stress profile in the Legendre polynomial basis, and then finding the coefficients of the basis from the measured strain data. For these near-surface residual stress measurements, all terms in the polynomial series were included (this is not the case when measuring through thickness stress distributions, as the zeroth and first order Legendre polynomials do not satisfy equilibrium). Taking x as the coordinate along the depth direction, the unknown residual stress profile $\sigma_{RS}(x)$ was written as a sum of Legendre polynomial terms $P_j(x)$, each with a corresponding amplitude A_j

$$\sigma_{RS}(x) = \sum_{i=0}^{m} A_j P_j(x) \tag{1}$$

where, m is the order of the highest term in the polynomial series. A solution of the equations of elasticity is then developed to relate the stress given by a particular basis function (with unit amplitude) $P_j(x)$ to strain at a near-slit gage location, as described below. If residual stress were given exactly by the basis function $P_j(x)$, the strain that would occur at cut depth a_i is provided by the elasticity solution. This strain is an element C_{ij} of a compliance matrix $[C]$ defined as

$$C_{ij} \equiv \varepsilon(a_i)\big|_{\sigma=P_j(x)}. \tag{2}$$

Solving the elasticity problem for all basis functions and all cut depths, and invoking the principle of elastic superposition, results in a linear system relating basis function amplitudes to strain as a function of cut depth

$$\varepsilon(a_i) = \sum_{j=0}^{m} C_{ij} A_j \tag{3}$$

or, using matrix notation

$$\{\varepsilon\} = [C]\{A\} \tag{4}$$

where the braces {•} denote a vector and the brackets [•] denote a matrix. Given this system, and strains measured experimentally during cutting, the amplitudes of the stress expansion are found by inversion of Equation (4) in a least squares sense

$$\{A\} = \left([C]^T[C]\right)^{-1}[C]^T\{\varepsilon_{meas}\} \tag{5}$$

where $\{\varepsilon_{meas}\}$ is a vector of measured strain data. With the amplitude vector $\{A\}$ determined, the stress state existing prior to cutting is obtained from Equation (1).

The polynomial order for the stress expansion m was selected for each set of measured strain data by considering the root mean square of the error between measured strain and the fitted strain of Equation (4), as a function of an assumed order of stress expansion m. Preliminary strain fits were computed for Legendre polynomial series of order zero through seven (i.e., m in Equations (1) and (3) was varied from 0 to 7, so that the polynomial series had one to eight terms). Low-order polynomial series generally exhibited high strain fit error, and increasing order decreased error only for a limited number of terms. The numerical condition of the inverted matrix in Equation (4) also becomes poor with increasing number of terms, so that error in experimental data can have a significant impact on the measured residual stress when an unduly large number of terms are taken in the stress expansion. Therefore, the number of terms must be selected to ensure a good fit to the measured strain while not needlessly amplifying experimental errors. In this work, the optimal order of polynomial series was determined by plotting the root mean square of the strain fit error versus series order m, and selecting the order at which the error reached a plateau [11]. Once the order was selected, single-standard-deviation error bounds were found for the residual stresses using statistical methods [12] based on a standard error in measured strain equal to the larger of the root mean square

strain fit error or the expected precision of the strain measurement system (3 με). Further aspects of order selection and error analysis for slitting were recently discussed by Hill and Lin [11].

A software program was used to determine the elements of the compliance matrix [*C*] of Equation (4). This program embodies the elasticity solution originally published by Cheng et al [13] with improved integration and geometric accuracy [14, 15]. The solution assumes a slit of finite width w is cut to depth a in a semi-infinite half-space, and provides strain averaged over a given gage length L_g, where the gage center lies a distance s from the slit center (Figure 1). Inputs to the software code included experimental values of L_g, s, w, and slit depths a_i, as well as the elastic properties of the aluminum, which were assumed to be E = 70.0 Gpa and ν = 0.33 [16]. Output of the software program was routed to a general matrix and data analysis package [17] for determination of the basis function amplitude vector $\{A\}$ and the measured residual stress, as well as for error analysis.

Experimental Details

Careful attention was paid to several aspects of the experiments. Strain gages had a gage length of 0.79 mm. A waterproofing system consisted of a layer of acrylic covered by a layer of paraffin wax and was applied to protect each strain gage. Both the adhesive and coatings were carefully masked during application to ensure at least 0.5 mm overlap of each coating, which was found to be crucial for reliable water resistance and accurate strain measurement. The slit center to gage center distance s was nominally 1.8 mm, which allowed room for these coatings.

Wire EDM was used for slitting to specified increments of depth. The final slit depth ranged from 1.3 to 2.0 mm, and slitting was performed while the specimen was bathed in de-ionized water. Initial experiments used 0.20 mm wire, which produced a slit approximately 0.25 mm wide, and strain data were gathered at nominal depth increments of 0.102 mm. In an attempt to improve the measurement resolution near the material surface, further experiments used 0.10 mm wire, which produced a slit approximately 0.12 mm wide. In these cases, the slit depth increments were 0.025 mm for the first six depths, 0.051 mm for the next seven depths, and then 0.102 mm for the remaining depths. Because the slit width was accounted for in the elastic solution, it was assumed to have a minimal impact on the measured stress. The smaller wire did allow smaller increments of depth to be cut, therefore improving near-surface resolution.

Transduced strain gage signals were produced by a commercial Wheatstone bridge and were recorded by hand. Cutting was halted prior to each strain reading to avoid interference from stray voltages produced by the cutting equipment.

After cutting was completed, the strain gage coatings were chemically and mechanically removed and measurement sites were examined under magnification. Digital images were captured at 50× optical magnification and had a resolution of approximately 530 pixels/mm (0.0019 mm/pixel). Digital photogrammetry was used to determine the slit width w, gage location s, and the final slit depth a_{max} for each measurement site. The measured slit width and gage location at each measurement site provided input to the stress computation. The measured maximum slit depth was used to adjust the intended slit depths to account for any offset between the depth axis of the EDM wire and the surface of the coupon. An offset was defined as the measured

maximum slit depth minus the intended maximum slit depth, and this offset was added to each intended slit depth to arrive at a set of adjusted slit depths, which were used in the stress computation.

Coupon and Measurement Site Descriptions

Seven coupons were used to address the five objectives described above. These coupons were cut from a single 7049 T73 aluminum forging. Shot peening was performed by a commercial provider (Metal Improvement Company Inc., Paramus, NJ, USA) to AMS-S-13165, using 0.48-0.71 mm cast steel shot, 200% coverage, and 0.010A-0.014A Almen intensity. Laser peening was performed on a novel Nd:glass, flash lamp pumped laser which incorporated SBS phase conjugation. The laser system was capable of an average power of 600 W, a pulse width of 10 to 100 ns, a pulse energy of up to 100 J, and a repetition rate of up to 6 Hz. Details on a similar laser system were previously reported by Dane et al [4] and a discussion of its use for LP was reported by Hammersley et al [6].

The LP parameters used for each coupon are listed in Table 1 (which also has a listing of the measurement sites on these coupons, described below). Initial measurements of residual stress were made on treated rectangular surfaces with planar dimensions 9.5x50 mm and with coupon thickness of 25 mm (coupons 5ST and 6LT). All other coupons were 9.5 mm thick and had planar dimensions at least 25x38 mm.

While the coupon geometries varied slightly, an effort was made to limit the effects of coupon and slit geometry on measured stress. The stress computation relies on an elastic solution for a slit in a semi-infinite half-space in plane strain, and several

geometric constraints were developed to approximate the geometry and boundary conditions of the elastic solution. The slit depth a_{max} was made small compared to the sample thickness to approximate an infinitely thick body (the greatest slit depth was 20% of the coupon thickness). The slit length was extended across the entire coupon and measurement locations were more than $2a_{max}$ along the slit from the coupon edges to approximate a plane strain condition. Multiple slits cut on the same coupon were remote from each other and from coupon edges to approximate a planar infinite body (the smallest perpendicular distance between slits or coupon edges was $6a_{max}$). In addition to these constraints, measurement sites were at least one laser spot size inside the peened area to assure that the full peening-induced stress fields were measured (except when specifically investigating stress near the edge of the peened area).

Residual stress profiles were measured at fifteen sites on the seven coupons. Example coupons, slit locations, and strain gage locations are shown in Figure 2. Measurement sites are defined by the locations of both the slit and the strain gage. For example, site 1 on coupon 4A (Figure 2(a)) is horizontally located at the strain gage, although the measurement is a weighted average of any residual stress variation that may exist along the line of the slit [18]. Site 1 is vertically located at the slit, because stress release occurs there, and no averaging occurs along this direction, providing a spatial resolution approximately equal to the slit width. A schematic representation of all measurement sites within the laser peening fields is shown in Figure 3. Note that the figure shows the sites relative to the laser spot layouts employed in peening and does not indicate the proximity of the sites to one another. Each site is denoted by a double ellipse,

where the center indicates the measurement location and the major axis lies along the slit direction, indicating the direction along which spatial averaging should be expected.

The collection of coupons and measurement sites (Table 1 and Figure 3) was capable of addressing the five objectives of the present work. Results at sites 0-S and 0-L allow for a general comparison between residual stress profiles due to SP and LP. Measurements at sites 1, 2, and 3 compare the effects of laser pulse fluence and laser spot size on the residual stress profiles. Comparison of results at site 0-L and site 1 shows the effect of a reduced second-layer pulse width (18 ns for site 0-L and 12 ns for site 1; the difference of 1 ns in the first pulse widths was assumed to be insignificant). Comparison of results for site 2 with those of site 7a shows the effect of layer overlap. Results at sites 4, 5, and 6 show the in-plane variation of the residual stress profile adjacent to the laser peened area. Results for sites 7a, 8a, 9a, and 11a reveal the in-plane variations of the residual stress profile within the peened area.

The effect of degraded or damaged optics was investigated by intentionally altering the spatial distribution of laser energy within the spots. With the current laser system [6], the most common problem is a reduced amount of laser energy in one corner of the square laser spot. To simulate such degradation under controlled conditions, one corner of the laser spot was intentionally attenuated (i.e., masked) and LP was performed in an otherwise normal manner. Coupon 7AT contained two laser peened areas, each 22.5 mm square, one area peened with normal spots and the other peened with attenuated spots. The attenuated area within the laser spot was 1.5x1.5 mm and is shown, together with the measurement sites within this peened area, in Figure 3(d). Comparison of results

at sites 10a and 11a with those at sites 12a and 13a shows the effect of a non-uniform spatial distribution of energy within the laser spots.

Results

The photogrammetric measurements for each measurement site are shown in Table 2. The nominal gage placement was 1.80 mm from the center of the slit, and the measured position varied from 1.51 mm to 2.03 mm. The differences between the intended and actual gage positions are due to inaccuracies in gage installation and in placement of coupon relative to the wire in the EDM machine. The slits exhibited typical amounts of over-cut observed for wire EDM, being 0.02 to 0.06 mm wider than the EDM wire (after accounting for differences in wire size). Cut depths varied from the intended depths by between 0.01 and 0.11 mm due to inaccuracies in placement of the coupon relative to the EDM wire. As stated above, measured gage positions, measured slit widths, and adjusted cut depths were used in the stress determination for each measurement site. The difference between the nominal and actual geometry had significant effects on the calculated stress, as discussed below.

Figure 4 shows measured strain data for sites 0-S and 0-L and the strain fit from the inverse elastic analysis. Although data and fits are shown for only two measurement sites, other sites exhibited similar trends in measured strain and similar agreement between measured and fitted strains. Note that the strain trends for these two measurement sites cannot be used to directly infer relative levels of residual stress since the geometry varied for these two measurement sites (Table 2) and this influences strain release due to slitting.

Stress profiles for SP and for variations in LP process parameters show interesting trends (Figure 5). Results at site 0-S compared with those at site 0-L indicate that compressive residual stress extended far deeper into the surface for LP than for SP (Figure 5(a)). These results also show that SP generated a larger compressive residual stress close to the surface for these laser settings. Decreasing the pulse width of the second-layer laser pulse from 18 to 12 ns increased the near-surface residual stress to a similar magnitude to that produced by SP (compare Figure 5(a) and (b)). Reducing the laser fluence from 60 to 45 J/cm^2 resulted in residual stress that was of similar magnitude near the surface, but that decreased more rapidly with distance from the surface (Figure 5(b)). Laser spot sizes of 3.2 and 5.0 mm produced very similar residual stress profiles (Figure 5(c)). Coupons treated with 10% and 50% layer overlap had similar levels of residual stress close to the surface, but the residual stress decreased more rapidly with depth for 10% overlap (Figure 5(d)).

The two most important characteristics of a stress profile may be the residual stress close to the surface and the depth that the compressive residual stress extends into the material. These two characteristics were quantified by interpolating the graphical results of Figure 5 at common points. For near-surface stress, residual stress at 0.10 mm was found. To quantify the depth of significant compressive residual stress, the depth where the residual stress first reached -50 MPa was found. With the exception of site 0-L, all sites had the same level of residual stress 0.10 mm from the surface, to within experimental uncertainty (Table 3). The compressive residual stress at the LP sites exceeded -50 MPa over a depth between 0.45 and 1.57 mm, which was a factor of 2.5 to 8.7 deeper than occurred for SP (Table 3).

Stress levels outside the peened area were significantly lower in magnitude than stresses within the peened area (Figure 6). Both near and below the surface, the magnitude of the residual stress decreased monotonically with distance from the laser peened area. No tensile residual stresses were measured outside the peened area. Measured residual stress at site 4 has more uncertainty near the surface than occurs at other measurement sites, due to difficulty in fitting the measured strain. It is suspected that gage coating material interfered with the EDM cutting at this site, so that initial slit depths were smaller than would otherwise occur. Even with the larger uncertainty at site 4, there was a significant decrease in residual stress outside the laser peened area.

Variations of the residual stress profile with in-plane position inside the peened area were limited to the near-surface region (Figure 7). The inset to Figure 7 summarizes the measurement sites for the four stress profiles presented in the figure. The highest surface residual stress was found at the edge of a layer two spot (site 9a), but because results were not available for all sites at shallow depths, it is not possible to make a definitive conclusion about which location had the highest or lowest stress at shallow depths. In the region between 0.10 and 0.20 mm, the largest stresses occurred at the center of a layer 2 spot (site 7a) with the difference between sites being as much as 100 MPa. Below 0.60 mm, all locations had similar stress profiles.

The effects of corner attenuation were also limited to the near-surface region (Figure 8). At the edge of a layer-two spot (sites 10a and 12a), residual stresses at depths less than 0.30 mm were significantly altered by corner attenuation, with the attenuated site having much lower stress close to the surface. At the center of a layer-one spot (sites 11a and 13a), near-surface residual stresses were unaffected by corner attenuation. At

depths greater than 0.30 mm, the stress profiles were similar at both sites, with or without corner attenuation.

Discussion

To investigate the variations of residual stress that may occur in laser peening, this paper presented measurements of the profiles of residual stress with depth from the surface for a variety of laser process parameters and at a variety of positions with respect to the laser spots. The major findings were that: 1) significant LP compressive residual stress extended far deeper into the material than SP compressive residual stress, 2) LP residual stress at a depth of 0.10 mm was less than or similar to that found for SP, depending on the laser parameters, 3) LP residual stresses at depths less than 0.20 mm were not significantly affected by most laser peening parameters, 4) higher fluence and larger layer overlap increased LP residual stresses at depths between 0.2 and 0.6 mm, 5) near-surface tensile residual stresses were not found adjacent to the laser peened area, and 6) variations in the residual stress profiles with in-plane position and variations due to degraded laser spots were limited to depths less than 0.60 mm. Before discussing the importance of these results, some choices made in planning this work and in reducing the experimental data should be discussed.

Although slitting was used in this study to measure residual stress, other techniques could have been used and may have had certain advantages. X-ray diffraction (XRD) might have been used to measure the in-plane surface residual stress variation, and might have been able to measure residual stress closer to the surface. Since the current results revealed in-plane spatial variations of LP residual stress near the surface, XRD would need to be carried out using a small x-ray spot to avoid in-plane averaging.

XRD could also have been used to measure the profile of residual stress with depth, using layer removal and correcting results for stress redistribution. However, the model commonly used to account for stress redistribution [19] assumes a uniform in-plane residual stress state. When designing this test program, errors due to the lack of in-plane stress state uniformity could not be estimated because the in-plane variations were unknown. Although the slitting method also suffers from averaging along the slit, it was attractive due to the lack of averaging normal to the slit. The slitting method also had the advantage of good performance for steep depth-wise stress gradients [10], whereas XRD can produce erroneous results in such cases [20].

It may be beneficial to combine XRD with slitting to measure the in-plane and in-depth variations of residual stress due to LP. In this study, there was difficulty in obtaining accurate results very close to the surface (depth less than about 0.07 mm) for two reasons. The first reason was that the largest numerical uncertainties for the slitting method occur near the beginning and end of the slit. The second reason was that repeatedly cutting to shallow depths was difficult because coatings used to protect the strain gage physically prevented the wire from contacting the coupon surface. Therefore, initial slits were of various depths. Although slit depth variations were accounted for in the stress computation, they did result in measurements at various depths and in an inability to obtain near-surface results in a few cases (e.g., site 8a). Despite the anticipated difficulties with XRD discussed above, some of these difficulties may be less significant at shallow depths. For example, the effect of in-plane stress variations on layer-removal corrections may be insignificant for depths that are small compared to the spatial scale of the in-plane stress variations. It may therefore be beneficial to employ

slitting and XRD at duplicate sites, and to combine diffraction results near the surface with slitting results at greater depths.

When formulating the compliance matrix [C], an analytical elasticity solution was employed, but it would have also been possible to use the finite element method. In finite element solutions, a small number of elements can be removed to simulate the extension of the slit, and slit-face tractions can be used to simulate the effect of the residual stress basis functions on near-slit strain (e.g., [10, 11]). To account for experimental variations in s, w, and a_i when using the finite element approach, one would need to adjust the finite element mesh for each variation of geometry. Alternatively, one could interpolate the results of a single finite element run to account for variations in s and a_i, assuming that small variations of w do not significantly affect the solution. A significant advantage of the analytical elasticity solution was that it could generate compliance matrices for different geometries more rapidly than a finite element mesh could be revised (i.e., s, w, and a_i were inputs to the software program invoking the solution and they could be easily changed).

The use of the measured strain gage position and offset slit depths had a significant effect on the computed residual stresses. To illustrate the effects of measured gage position and offset slit depths, the stress computation was repeated for two measurement sites. For site 0-S, the analysis was repeated using the intended gage position s = 1.8 mm and the offset slit depths. Residual stresses at all depths were affected, with the largest differences near the surface (Figure 9). For site 0-L, the analysis was repeated using the intended slit depths and the measured value of s. Near-surface stresses were again significantly affected (Figure 10). It is therefore advisable to measure

gage position and final cut depths following slitting experiments, and for the measurements to be included in stress computations.

Several of the key findings mentioned above may have important implications for potential LP applications. Compared with SP, compressive surface residual stresses due to LP were of similar magnitude near the surface (Table 3) and extended far deeper into the surface of the component (Table 3, Figure 5(a)). The greater depth of compressive residual stress that occurred with LP should serve to enhance fatigue performance to a greater degree than occurs with SP. In fact, enhanced fatigue performance has been shown for laser peened coupons in a number of fatigue studies involving SP and LP [3, 6, 8, 21].

Near-surface residual stresses due to LP were significantly affected by only a single LP parameter. Residual stress at depths less than 0.20 mm were significantly increased when the second-layer pulse width was decreased from 18 to 12 ns (compare results at site 0-L and site 1 in Figure 5 and Table 3). Since this made the near-surface stress as large as that found for SP, the shorter second-layer pulse duration was advantageous. All other laser parameter variations produced little change in the near-surface stress (Figure 5 and Table 3), indicating that near-surface stress was robust to variations of laser fluence, spot size, and layer overlap.

Residual stresses at depths between 0.20 mm and 0.60 mm were significantly affected by both laser fluence and layer overlap. Larger compressive residual stresses were found in this depth range with increased laser fluence and with increased layer overlap. The amount of the residual stress increase for both parameters was greatest near a depth of 0.40 mm and was approximately 75 MPa in each case.

The variations in the residual stress profiles caused by the variations of LP parameters should have implications on the fatigue performance of peened components. Improvements in fatigue life due to surface treatments like SP and LP are mainly due to the compressive residual stresses they impart. When considering the effects of surface treatment on fatigue life, it is useful to consider the phases of crack initiation and crack propagation separately. Fatigue crack initiation usually takes place very near the surface, and is therefore most influenced by the magnitude of the near-surface residual stress [22]. Since the variations of laser fluence, overlap, and spot size investigated here did not produce a significant change in the level of residual stress at depths less than 0.20 mm, LP should be a robust method for increasing lifetime to fatigue crack initiation. One possibly confounding issue, however, is that fatigue cracks may initiate away from the surface when high levels of compressive surface stress exist in a shallow layer [23, 24].

The influence of surface treatment on fatigue crack propagation is due to the contribution of residual stress to the total stress intensity factor (which is also affected by the applied cyclic loading). This contribution is most often quantified using the weight function [25], which shows that the contribution is linearly affected by the residual stress magnitude and non-linearly affected by the shape of the residual stress profile. While a weight-function analysis is beyond the scope of the present work, it can be stated unequivocally that residual stresses resulting from LP with higher fluence and larger layer overlap would have a larger contribution to the stress intensity factor because they have higher levels of compressive stress (Figure 5(b) and (d)). Components peened at higher fluence and larger overlap should therefore exhibit a longer crack propagation lifetime.

The effects of the LP variations on total fatigue life may depend on the level of loading. For highly loaded components that exhibit short to intermediate fatigue lifetimes (e.g., 10^3 to 10^5 cycles), life is mostly spent in crack initiation [26, 27]. The LP process variations should therefore not play a significant role in fatigue life improvements offered by LP for highly loaded components. For components carrying lower loads and exhibiting long lifetimes ($> 10^6$ cycles), a significant portion of the life is spent in crack propagation [26, 27]. The LP variations may therefore have a significant effect on fatigue life improvements for lightly loaded components. Since the effects of the LP variations are expected to be different for the crack initiation and crack propagation phases, their impacts on total fatigue life should depend on the level of loading. A fatigue test program would be required to validate this hypothesis, but such a program would likely require a large number of coupons to understand the effects of LP process variations in the presence of the stochastic nature of the fatigue process.

The fact that tensile surface residual stress was not found adjacent to the laser peened area suggests that LP should not have detrimental effects on fatigue performance. While compressive residual stress near the surface is desirable, tensile residual stress must exist at some other locations within the body to satisfy equilibrium. The results here suggest that the residual stress component perpendicular to the edge of the peened area is compressive on the surface adjacent to a laser peened area, suggesting that tensile stresses are limited to the component interior. Interior tensile residual stresses are of less concern because crack initiation is mainly a near-surface phenomenon due to the presence of surface roughness, oxidizing atmosphere, and higher stresses (when bending or torsion loadings exist) [22, 26]. However, the results here may not be representative of what may

occur in other geometries or for other residual stress components. Other research has investigated the residual stress component parallel to the edge of the peening field and found it to be tensile near the surface, outside the peened region [28]. The effect of residual stresses outside the peened region on fatigue performance would therefore depend on the direction of the applied stress in relation to the edge of the peened area. When the applied stress is perpendicular to the edge of the peened area, residual stresses outside the peened region should be of little concern.

The variations of the residual stress profiles with in-plane position were limited to depths less than 0.60 mm. These measurements were a first attempt to quantify the variation of the residual stress profile in the peened area. Three of the locations investigated lie along the boundary between two layer-one spots, starting at the center of a layer-two spot (site 7a, Figure 7 inset) and progressing out to the edge of a layer-two spot (sites 8a and 9a). At a depth of 0.10 mm, the results indicate that higher compressive residual stress existed at the center of a layer-two spot (site 7a) than at the edge (site 9a). Residual stress at a depth of 0.10 mm and at the center of a layer-one spot (site 11a) fell between those at the other sites. Results at shallower depths were not available at all sites due to the experimental difficulties described above. In summary, the results show that in-plane variations of the residual stress profile do exist within the laser peened area, and this suggests that fatigue cracks may initiate and grow at preferred locations (i.e., at locations of lower stress magnitude). It would therefore be of value for LP fatigue test programs to include a component of fractography to determine whether in-plane variations of residual stress lead to preferred sites for crack initiation and growth. This

information would also provide supporting evidence for the stress variations reported here, which have been found from a limited number of experimental measurements.

The variations of residual stress due to degraded laser spots were limited to shallow depths. Near-surface residual stress at the edge of a layer-two spot was significantly less when laser spots had attenuated corners (compare site 10a with site 12a, Figure 8). When the corner was attenuated, the level of near-surface stress at this location was significantly less than at any other location peened with normal laser spots (Figures 5 and 7). The fact that corner attenuation had little effect on residual stress at one location in the laser peened field (compare sites 11a and 13a), but a marked effect at another location (compare sites 10a and 12a) is non-intuitive. Future work should be directed at verifying this result, since the current work presents only limited experimental results. If attenuated laser spots lead to a reduced level of near-surface stress, this may lead to a preferred location for crack initiation, as just described. It therefore would be advisable to take steps to ensure a uniform spatial distribution of energy within the laser spots, which was a particular advantage of the laser system employed in this work [4].

Acknowledgements

Thanks are due to Fritz Harris of the Metal Improvement Company Inc. for helpful discussions, to John Halpin of Lawrence Livermore National Laboratory (LLNL) for laser engineering, to Laurie Lane of LLNL for laser peening, and to Greg Cook of Woodland Precision Technology for EDM. Michael B. Prime of the Los Alamos National Laboratory generously provided software implementing the elastic solution for strain near a finite width slit. UC Davis received financial support from Metal Improvement

Company Inc. and LLNL received financial support from the National Center for Manufacturing Sciences (USA).

References

[1] P. Peyre, X. Scherpereel, L. Berthe, C. Carboni, R. Fabbro, G. Beranger, C. Lemaitre, Mater. Sci. Eng. A280 (2000) 294.

[2] P. K. Sharp, G. Clark, The Effect of Peening on the Fatigue Life of 7050 Aluminum Alloy, Defence Science & Technology Organisation, Victoria, Australia, 2001

[3] P. Peyre, R. Fabbro, P. Merrien, H. P. Lieurade, Mater. Sci. Eng. A210 (1996) 102.

[4] C. B. Dane, L. E. Zapata, W. A. Neuman, M. A. Norton, L. A. Hackel, IEEE J. Quantum Electron. 31 (1995) 148.

[5] C. B. Dane, L. A. Hackel, J. M. Halpin, J. Daly, J. Harrisson, F. Harris, High-throughput laser peening of metals using a high-average-power Nd:glass laser system, in: S. Nakai, L.A. Hackel, W.C. Solomon (Eds.), High-Power Lasers In Civil Engineering and Architecture, Society of Photo-Optical Instrumentation Engineers, Bellingham, WA, 2000, pp. 211-221.

[6] G. Hammersley, L. A. Hackel, F. Harris, Opt. Lasers Eng. 34 (2000) 327.

[7] P. R. Smith, M. J. Shepard, P. S. Prevéy, A. H. Clauer, J. Mater. Eng. Perform. 9 (2000) 33.

[8] P. Peyre, P. Merrien, H. P. Lieurade, R. Fabbro, Surf. Eng. 11 (1995) 47.

[9] X. Scherpereel, P. Peyre, R. Fabbro, G. Lederer, N. Celati, Modification of electrochemical properties of stainless steel by Laser Shock Processing, in: M.H. Aliabadi, C.A. Brebbia (Eds.), Proceedings of the International Conference on Computer Methods and Experimental Measurements for Surface Treatment Effects, WIT Press, Southampton, UK, 1997, pp. 83-92.

[10] M. B. Prime, Appl. Mech. Rev. 52 (1999) 75.

[11] M. R. Hill, W. Lin, J. Eng. Mater. Technol. 124 (2002) 185.

[12] P. R. Bevington, D. K. Robinson, Data Reduction and Error Analysis for the Physical Sciences, 2nd ed, McGraw-Hill, New York, 1992, pp. 115-138.

[13] W. Cheng, I. Finnie, J. Eng. Mater. Technol. 115 (1993) 220.

[14] M. B. Prime, I. Finnie, J. Eng. Mater. Technol. 118 (1996) 410.

[15] W. Cheng, I. Finnie, M. Gremaud, M. B. Prime, J. Eng. Mater. Technol. 116 (1994) 1.

[16] J. R. Davis (Ed.), ASM Specialty Handbook - Aluminum and Aluminum Alloys, ASM International, Materials Park, OH, 1993, p. 695.

[17] MATLAB, 5.3.0.10183 (R11), The MathWorks, Inc, Natick, MA, 1999.

[18] W. Cheng, I. Finnie, Ö. Vardar, J. Eng. Mater. Technol. 113 (1991) 199.

[19] M. G. Moore, W. P. Evans, SAE Transact. 66 (1958) 340.

[20] P. S. Prevéy, X-ray diffraction characterization of residual stresses produced by shot peening, in: A. Niku-Lari (Ed.) Shot Peening Theory and Application, IITT-International, Gournay-Sur-Marne, France, 1990, pp. 81-93.

[21] A. H. Clauer, Laser Shock Peening for Fatigue Resistance, in: J.K. Gregory, H.J. Rack, D. Eylon (Eds.), Surface Performance of Titanium, TMS, Warrendale, PA, 1996, pp. 217-230.

[22] J. O. Almen, P. H. Black, Residual Stresses and Fatigue in Metals, McGraw-Hill Book Company, Inc, New York, NY, 1963, p. 59.

[23] D. W. Hammond, S. A. Meguid, Eng. Fract. Mech. 37 (1990) 373.

[24] M. Larsson, A. Melander, R. Blom, S. Preston, Mater. Sci. Technol. 7 (1991) 998.

[25] A. P. Parker, Stress intensity factors, crack profiles, and fatigue crack growth rates in residual stress fields, in: J.B. Wheeler (Ed.) Residual Stress Effects in Fatigue, ASTM STP 776, American Society for Testing and Materials, Philadelphia, PA, 1982, pp. 13-31.

[26] D. K. Benson, Surface treatments for fatigue strengthening, Achievement of High Fatigue Resistance in Metals and Alloys, ASTM STP 467, American Society for Testing and Materials, Baltimore, MD, 1970, pp. 188-208.

[27] B. R. Sridhar, K. Ramachandra, K. A. Padmanabhan, J. Mater. Sci. 31 (1996) 5953.

[28] J. J. Ruschau, R. John, S. R. Thompson, T. Nicholas, J. Eng. Mater. Technol. 121 (1999) 321.

Tables

Coupon	Site	Fluence (J/cm^2)	Pulse width		Size (mm)	Overlap (%)	Purpose or Effect
			1 (ns)	2 (ns)			
5ST	0-S	--	--	--	--	--	SP residual stress
6LT	0-L	60	18	18	5	10	Compare LP to SP
4A	1	60	17	12	5	10	Shortened second pulse
	2	45	17	12	5	10	Reduced laser energy
4AT	3	60	17	12	3.2	10	Reduced spot size
6AT	4	45	17	12	5	50	At edge of LP area
	5	45	17	12	5	50	1.25 mm beyond LP area
	6	45	17	12	5	50	2.5 mm beyond LP area
6A	7a	45	17	12	5	50	Center of layer 2 spot
	8a	45	17	12	5	50	In layer 2 spot
	9a	45	17	12	5	50	Edge of layer 2 spot
7AT	10a	45	17	12	5	50	Clean, edge of layer 2 spot
	11a	45	17	12	5	50	Clean, center of layer 1 spot
	12a	45	17	12	5	50	Attenuated, edge of layer 2 spot
	13a	45	17	12	5	50	Attenuated, center of layer 1 spot

Table 1: Experimental coupons and strain gages

Coupon	Site	s (mm)	w (mm)	a_{max} (mm)
5ST	0-S	1.51	0.25	1.41
6LT	0-L	1.73	0.25	1.28
4A	1	1.65	0.12	2.00
	2	1.63	0.12	2.03
4AT	3	2.03	0.13	2.02
6AT	4	1.91	0.15	2.02
	5	1.95	0.15	2.04
	6	1.93	0.16	2.07
6A	7a	1.54	0.13	2.02
	8a	1.69	0.12	2.07
	9a	1.71	0.13	2.01
7AT	10a	1.78	0.12	2.01
	11a	1.77	0.11	2.01
	12a	1.69	0.13	2.02
	13a	1.85	0.12	2.02

Table 2: Gage position s, slit width w, and cut depth a_{max} for each measurement site

Site	Condition	Near Surface Residual Stress (MPa)	Depth of Compressive Residual Stress (mm)
0-S	Shot Peened	-256 ± 9	0.18
0-L	60 J/cm^2 18 ns 18 ns	-188 ± 9	> 1.30
1	60 J/cm^2 17 ns 12 ns	-263 ± 29	1.33
2	45 J/cm^2 17 ns 12ns	-263 ± 21	0.45
3	60 J/cm^2 17 ns 12ns (3.2 mm)	-253 ± 12	1.57

Table 3: Summary of near surface residual stress and depth of compressive residual stress

Figures

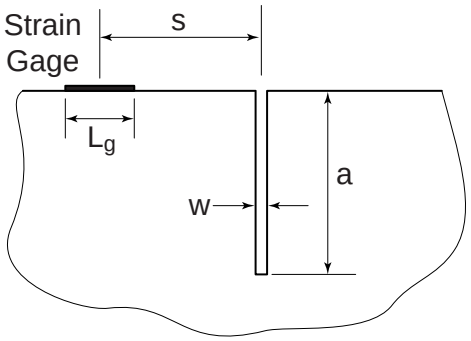

Figure 1: Strain gage installation schematic

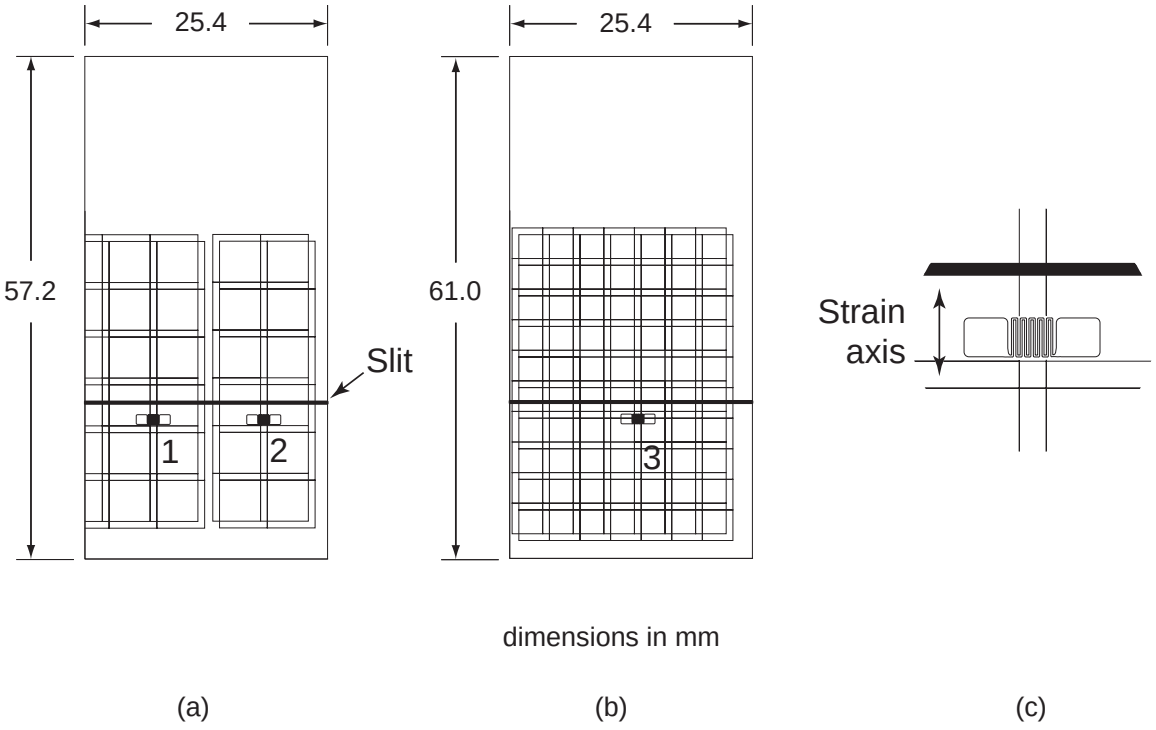

Figure 2: Examples of laser peened coupons, slits, and strain gage locations: (a) coupon 4A having two levels of laser fluence (left side 60 J/cm^2, right side 45 J/cm^2), (b) coupon 4AT with smaller laser spots, and (c) larger view of slit and strain gage

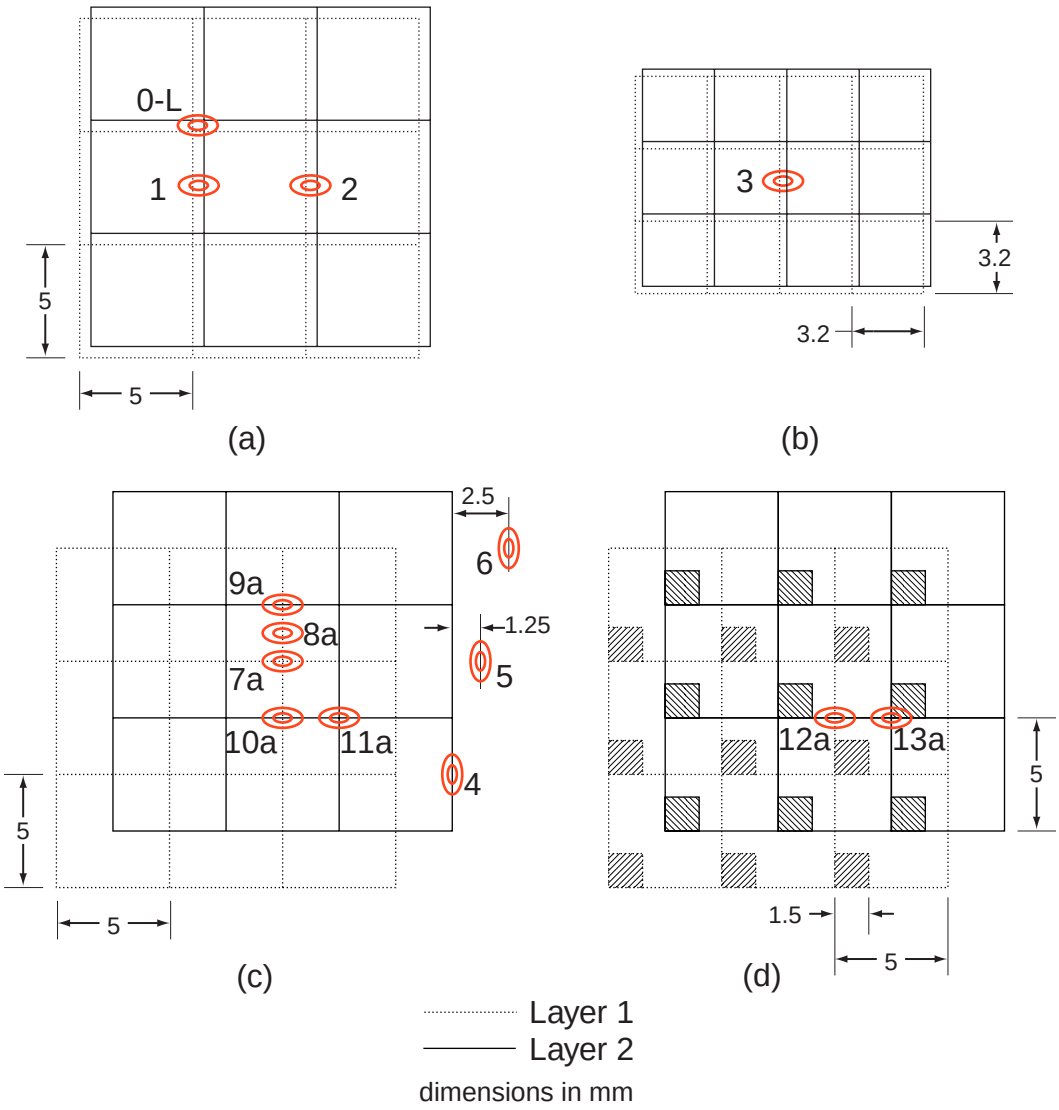

Figure 3: All measurement sites relative to peening fields: (a) 10% overlap and 5x5 mm spot, (b) 10% overlap and 3.2x3.2 mm spot, (c) 50% overlap and 5x5 mm spot, (d) 50% overlap and 5x5 mm spot with a 1.5x1.5 mm corner attenuation as indicated with cross hatching

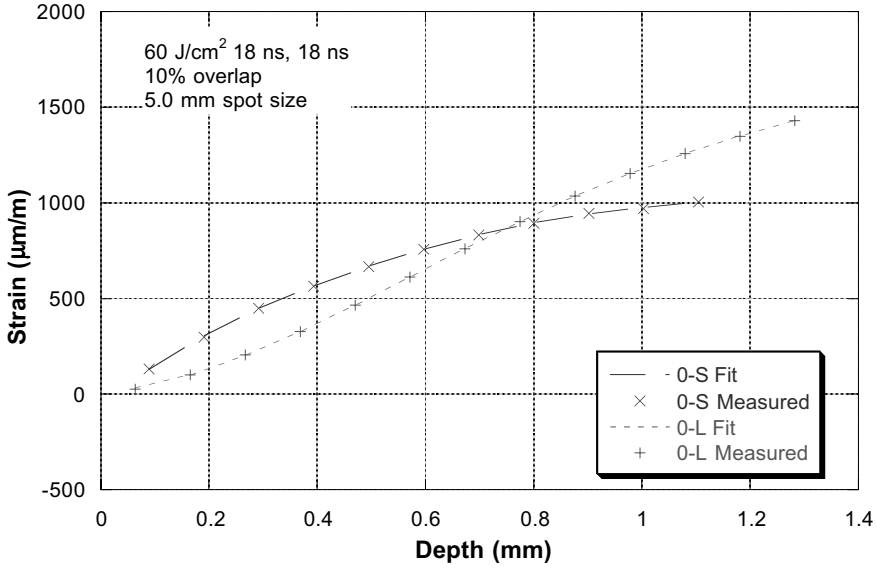

Figure 4: Measured strain and strain fits for sites 0-S and 0-L

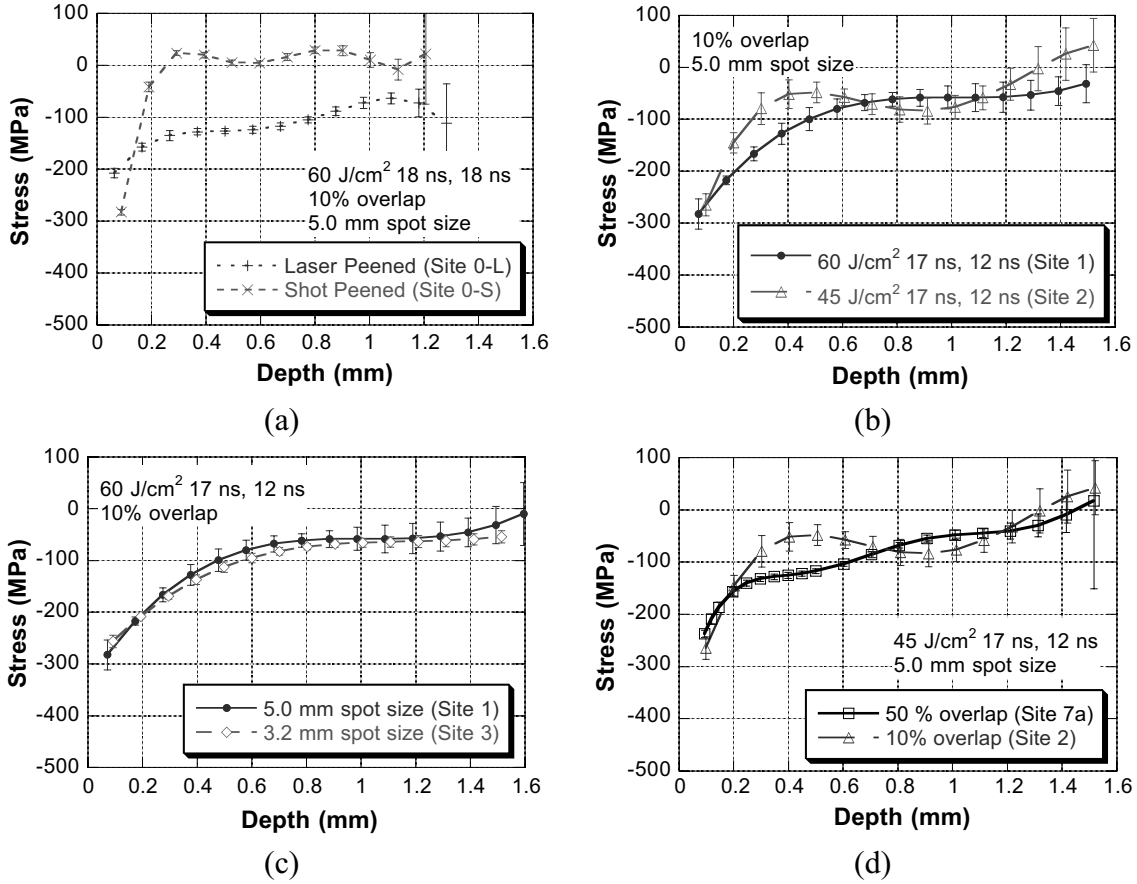

Figure 5: Comparison of peening processes: (a) SP vs. LP (b) effect of energy density; (c) effect of spot size; (d) effect of layer overlap

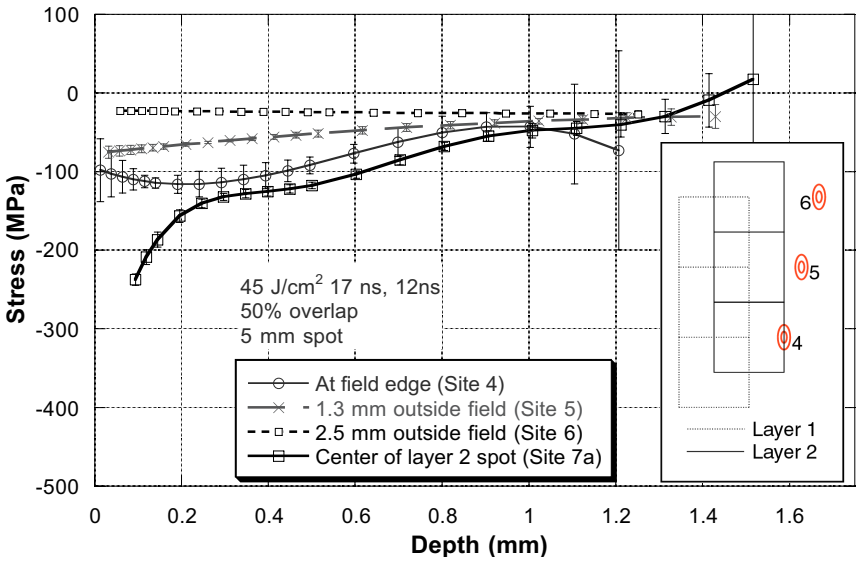

Figure 6: Residual stress adjacent to a laser peened area

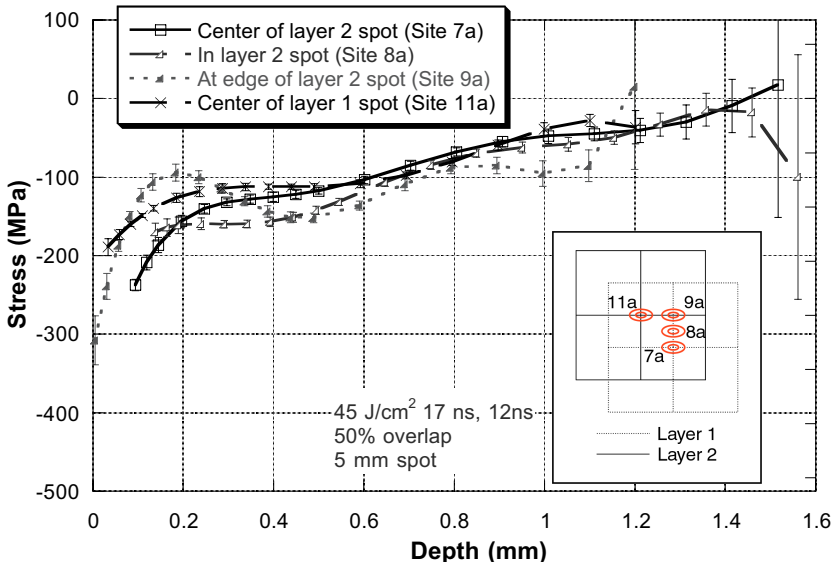

Figure 7: In-plane variations of the residual stress profile

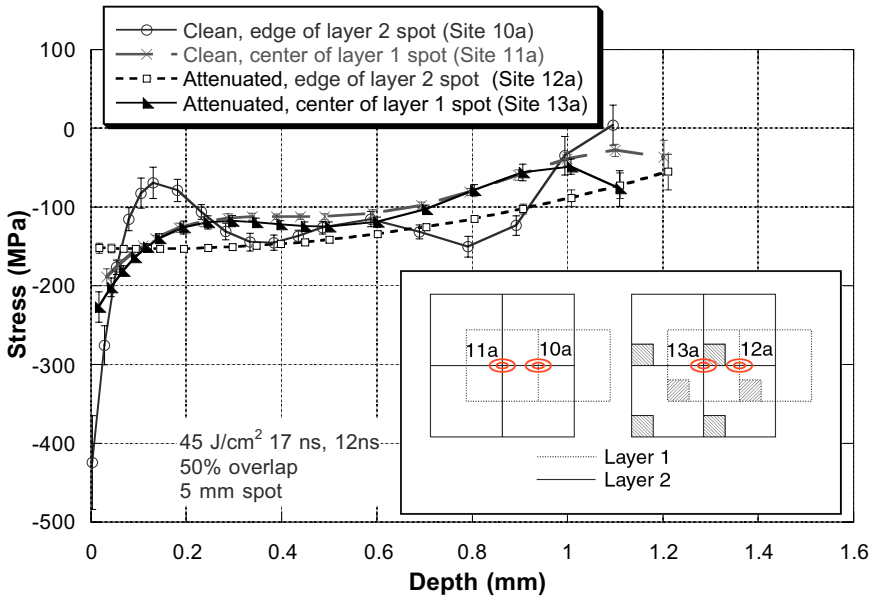

Figure 8: Comparison of residual stress profiles with and without corner attenuation

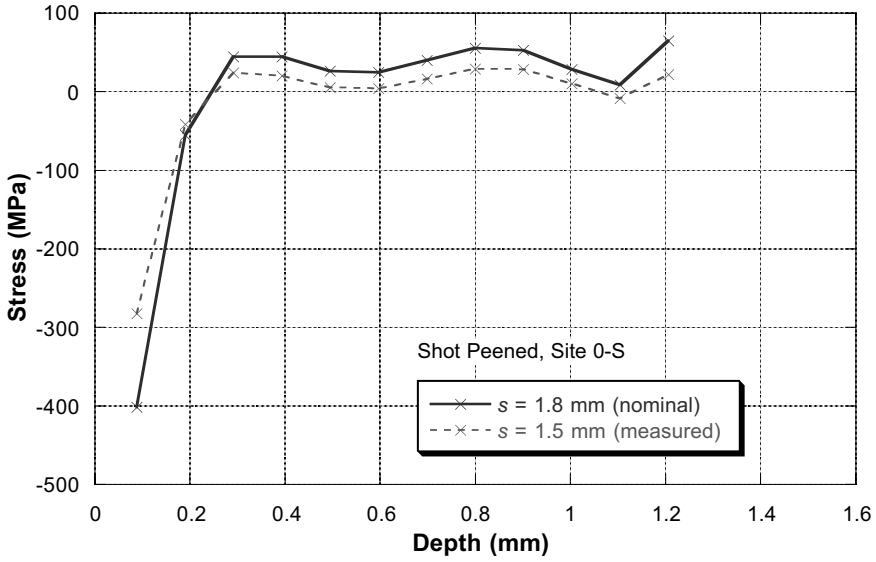

Figure 9: Residual stress for site 0-S computed with nominal and measured gage position

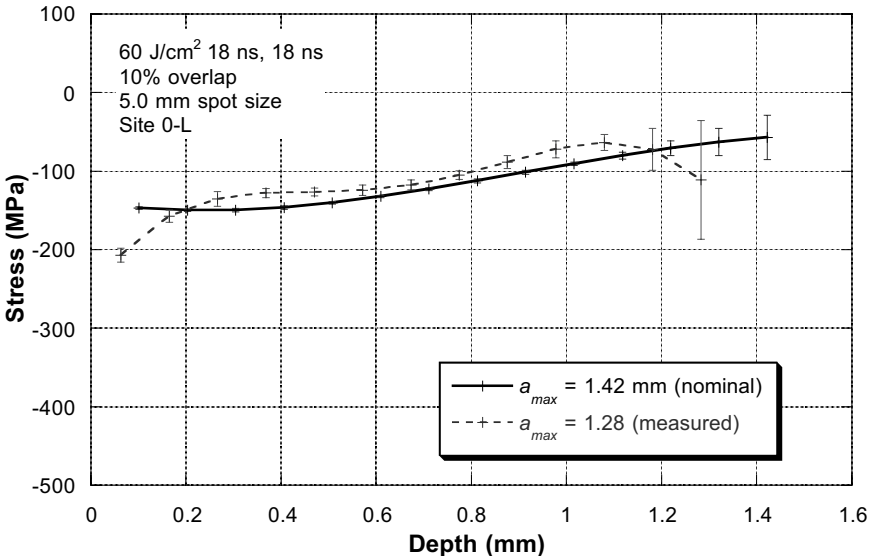

Figure 10: Residual stress for site 0-L computed with nominal and measured maximum cut depth